Journal of Magnetic Resonance 207 (2010) 59–68

Contents lists available at ScienceDirect

Journal of Magnetic Resonance

journal homepage: www.elsevier.com/locate/jmr

An electromagnetic reverse method of coil sensitivity mapping for parallel MRI – Theoretical framework

Jin Jin [a], Feng Liu [a], Ewald Weber [a], Yu Li [a], Stuart Crozier [b,*]

[a] MedTeQ Centre, The School of Information Technology and Electrical Engineering, The University of Queensland St. Lucia, Brisbane, Qld 4072, Australia
[b] Biomedical Engineering Director, MedTeQ Centre, The School of Information Technology and Electrical Engineering, The University of Queensland, St. Lucia, Brisbane, Qld 4072, Australia

ARTICLE INFO

Article history:
Received 17 March 2010
Revised 2 August 2010
Available online 17 August 2010

Keywords:
Parallel imaging
Sensitivity
Mapping
Reconstruction

ABSTRACT

In this paper, a novel sensitivity mapping method is proposed for the image domain parallel MRI (pMRI) technique. Instead of refining raw sensitivity maps by means of conventional image processing operations such as polynomial fitting, the presented method determines coil sensitivity profiles through an iterative optimization process. During the algorithm implementation the optimization cost function is defined as the difference between the raw sensitivity profile and the desired profile. The minimization is governed by the physics of low-frequency electromagnetic and reciprocity theories. The performance of the method was theoretically investigated and compared with that of a traditional polynomial fitting, against a range of system noise levels. It was found that, the new method produces high-fidelity sensitivity profiles with noise amplitudes, measured as root mean square deviation an order of magnitude less than that of the polynomial fitting method. Using the sensitivity profiles generated by our method, SENSE (sensitivity encoding) reconstructions produce significantly less image artefacts than conventional methods. The successful implementation of this method has far-reaching implications that accurate sensitivity mapping is not only important for parallel reconstruction, but also essential for its transmission analogy, such as Transmit SENSE.

1. Introduction

In this paper, a novel sensitivity mapping method is proposed for image domain parallel reconstruction algorithms. Instead of refining raw sensitivity maps by means of image processing operations or polynomial fitting procedures, the presented method determines the coil sensitivity profiles by resorting to physics of electromagnetics.

Parallel imaging (PI) is used widely in advanced MRI applications. Complementing gradient encoding schemes, spatial encoding by means of distinct coil sensitivities is incorporated into PI to improve scan speed and coverage [1]. Sensitivity encoding (SENSE) [2,3] and generalized auto calibrating partially parallel acquisitions (GRAPPA) [4] methods continue to be the two most popular PI methods. SENSE represents a class of image domain methods [2,5,6], in which the reconstruction coefficients are calculated in the image domain, whereas GRAPPA and its variants [4,7–9], known as spatial-frequency domain methods, acquire reconstruction coefficients in K-space. These seemingly distinct classes of methods can be seen as different approaches to solving the same set of linear equations of inverse problems [10]. A distinction between the two approaches is that image domain methods require an explicit extraction of the coil sensitivities, whereas sensitivity information is involved in spatial-frequency domain methods implicitly. Despite the extra work of sensitivity mapping, image domain methods are often preferred since they can provide accurate solutions to the inverse problem and achieve an optimal reconstruction [11] provided the sensitivities are known exactly, whereas GRAPPA gives a solution based on approximating the linear combination coefficients for the repopulation of the missing K-space lines. Furthermore, SENSE can outperform GRAPPA in some imaging scenarios since it allows greater opportunity to control reconstruction quality through regularization [12]. Traditionally, the sensitivity profile of a coil is defined by the division between a coil image and a uniform reference image, which are obtained from reference scans of a body coil or sum-of-squares of surface coil arrays [2]. This raw sensitivity profile is then refined by two-dimensional polynomial fitting [2]. Dynamic self-calibrating methods [13] have been developed to deal with sensitivity misregistration that can result from the traditional methods. However, the truncation in the spatial-frequency domain of the dynamic

* Corresponding author. Fax: +61 (0)7 3365 4999.
E-mail addresses: jinjin@itee.uq.edu.au (J. Jin), feng@itee.uq.edu.au (F. Liu), ewald@itee.uq.edu.au (E. Weber), yuli@itee.uq.edu.au (Y. Li), stuart@itee.uq.edu.au (S. Crozier).

1090-7807/$ - see front matter Crown Copyright © 2010 Published by Elsevier Inc. All rights reserved.
doi:10.1016/j.jmr.2010.08.009

methods causes Gibbs phenomena. Apodization, wavelet de-noising techniques [14] and polynomial fitting [2,15] have been used to reduce Gibbs ringing, however, these methods all have difficulty cancelling the ringing errors [15].

Here we propose a novel sensitivity mapping method based on the theory of reciprocity [16,17], which allows the evaluation of the receiving sensitivity from transmitting B_1^+ field. In this approach, the measured raw sensitivity profile is first used to inversely determine the coil array geometry by solving the associated electromagnetic problem. With the coil array information known, the coil sensitivity profile can then be calculated as the B_1 reception field (B_1^-). In this proof-of-concept research, we will focus on low fields ($B_0 \leqslant 1.5$T) in the so-called near-field regime, where the RF wavelength λ is much larger than the object and the coil array. As the problem is reduced to quasi-static in this regime, the set of four Maxwell's equations are reduced to Ampere's Law for the calculation of magnetic field. As a result, the reciprocal magnetic field (B_1^-) can be calculated by Biot–Savart integration derived from Ampere's law with quasi-static limit, since the RF field is weakly distorted by the object being scanned [1,18,19]. The proposed method will be demonstrated in two cases: the sensitivity mapping for a single coil element and the sensitivity mapping for an element in a four-element array. A performance comparison of the proposed and the traditional polynomial fitting method will be carried out, for both scenarios.

2. Methods

Similar to our recent work on exposure evaluations by reverse-engineering of gradient coils [20], the geometry of a typical radio frequency (RF) coil can be inversely determined from the measured magnetic field information. In low field cases, this reverse method is made possible by the reasons that the RF coil can be represented by a mathematical model using a few model descriptors. Then, using the principle of reciprocity [16,17] we are able to reproduce the measured B_1 field propagation using Biot–Savart integration with steady current flowing in the coil element. With appropriate parameterization, an optimization algorithm can then be used to attain the values of descriptors representing the RF coil geometry.

Firstly, this work will review the traditional sensitivity mapping method, which serves as a basis for evaluation and comparison. Using the two sensitivity mapping case studies, we then derive a framework for acquiring sensitivity profiles from a raw sensitivity map and limited information of coil array geometry. Case I will show, in the simplest way, how a noisy sensitivity profile is denoised by the new method. In Case II, the method is extended to handle coil arrays. In these studies, noise is introduced into the system in a controlled manner.

2.1. Conventional image-domain coil sensitivity mapping

Noise is inevitably found in any MR image and consequently in the measured sensitivity maps. One of the conventional methods for sensitivity mapping and noise mitigation was introduced by Pruessmann et al. [2], alongside the SENSE method. The procedure is illustrated in Fig. 1. Here a coil image (A) is divided by a uniform reference image (B) to produce a raw sensitivity map (C). However, noise in the raw sensitivity map, augmented by the division, is usually a serious issue during this procedure, particularly in areas with low proton density [21], such as the 'holes' which appeared in Fig. 1C. To mitigate contaminating noise, profile C is masked by a binary profile, which is obtained by applying a threshold on the uniform reference image (B). A profile of sensitivity information within the reliable region (D) is thus obtained. The extrapolation zone (E) is produced by a morphological region-growing approach. A two-dimensional local polynomial fit, based upon the assumption that coil sensitivity has a slowly changing profile, is performed on the extrapolation zone to acquire the refined sensitivity map (F).

2.2. Case I – single coil element

A sensitivity profile is a function of the coil geometry, object characteristics and the resonant frequency. The single coil model shown in Fig. 2A consists of only one element of a typical RF coil array and a spherical phantom. The coil element is specified by a few descriptors: γ representing the opening of the coil element, α representing the azimuth angle with respect to 0° of the cylindrical coordinate system and $\bar{I}$ representing the resonant current. Using these parameters, the functional dependence of the magnetic field can be described as:

$$\boldsymbol{B}_0 = \mathcal{F}_0(\gamma, \alpha, \bar{I}) \tag{1}$$

where the sensitivity profile $\boldsymbol{B}_0$ is a function of parameters γ, α, and $\bar{I}$.

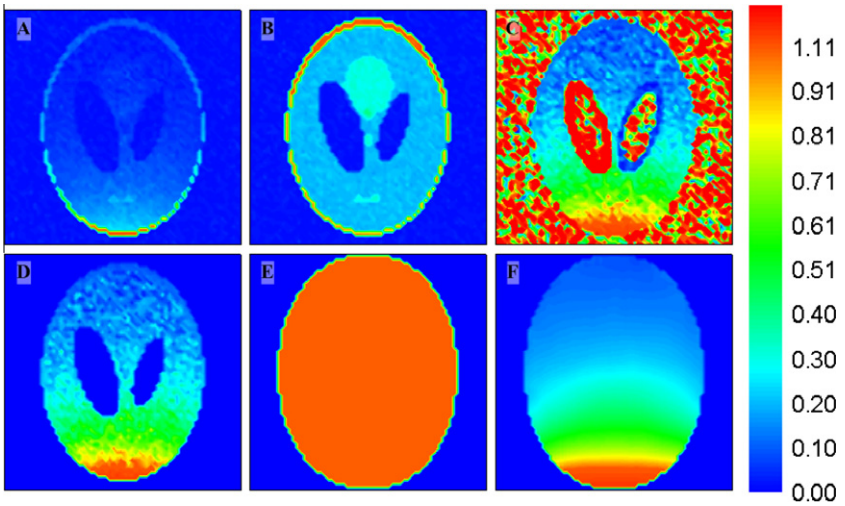

Fig. 1. Coil sensitivity mapping procedure proposed by Prussmann et al. An array image (A) is divided by a body coil image (B) to produce a raw sensitivity map (C), which is then masked to obtain a profile with only reliable sensitivity information (D). The extrapolation zone (E) is produced by a morphological region growing approach. Two-dimensional local polynomial fit is performed to acquire the sensitivity map (F).

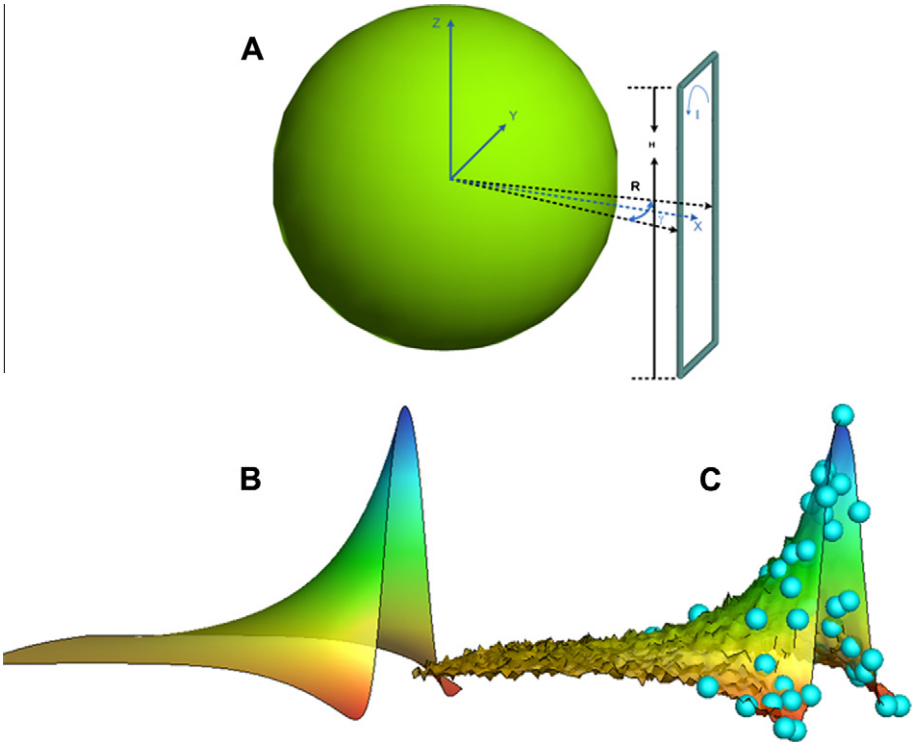

Fig. 2. A. Coil Geometry and Model Descriptors. I represents the resonant current. γ is the opening angle of the coil. α is the azimuth angle with respect to x-axis. (α equals zero in current case) The field-of-field (FOV) is located in the centre slice ($Z = 0$) of the spherical phantom. R is the distance from the centre of FOV to the vertical wires. H is the length of the vertical wires. (B): The simulated sensitivity profile obtained from FOV. C: The noised-added sensitivity profile, with sampling points representing sensitivity characteristics (blue dots). (For interpretation of the references to colour in this figure legend, the reader is referred to the web version of this article.)

Clearly, an accurate description of this functional dependence is crucial for the proposed method. The field has dependence on coil array geometry, specified by γ and α, current $\bar{I}$ of the coil, as well as the resonance frequency of the MR system. At low fields, the quasi-static magnetic approximation applies. A set of four Maxwell's Equations are reduced to Ampere's Law with steady current for the calculation of magnetic field strength using Eq. (1). By virtue of the principle of reciprocity [16,17], the sensitivity profile can be obtained from the (hypothetical) RF field as long as the function $\mathcal{F}_0$ can successfully describe the dependence of $\boldsymbol{B}_0$ on the parameters. An optimization process can be utilized to determine a set of parameter values that generate the least square fit to the measured profile. A general form of the optimization cost function that quantifies the discrepancy between the hypothetical and the measured field is:

$$\boldsymbol{\Phi} = (\boldsymbol{B_0} - \boldsymbol{B'}) \times (\boldsymbol{B_0} - \boldsymbol{B'})^H \tag{2}$$

where $\boldsymbol{B_0}$ is the hypothetical field with dependence on γ, α, $\bar{I}$ through function $\mathcal{F}_0$; and $\boldsymbol{B'}$ is the measured sensitivity profile; and the superscript H denotes conjugate transpose.

Case I is a simplified scenario, which shows how a noisy sensitivity profile is de-noised by the new method. A scheme was designed to incorporate the noise into the system in a quantitative manner. Firstly, a noise-free sensitivity profile (Fig. 2B) was calculated by employing electromagnetic simulation software FEKO (EMSS, SA). The coil element was numerically tuned to resonate at 64 MHz and the magnetic field in X–Y plane was studied at $Z = 0$. Granted by the principle of reciprocity [16], the coil sensitivity profile (B_1^-) was readily available once the B_1^+ field was obtained. In this study, the model parameters are as follows: phantom relative permeability $\varepsilon_r = 30$, conductivity $\sigma_1 = 0.3$S/m, mass density $\rho_1 = 1030$ kg/m^3, coil height $h = 90$ mm, radius $R = 37.6$ mm, $\alpha = 0°$ and $\gamma = 35°$. Secondly, various amounts of Gaussian noise with amplitudes ranging from -50 dB to -30 dB, with respect to signal, were added to the, otherwise noise-free, FEKO simulation results. Signal amplitude was derived using the following procedure (real and imaginary parts of the simulated profile are examined independently): a region of relatively high amplitude was chosen, the average of which was taken as the signal amplitude. Noise amplitude was determined according to Eq. (3), which was derived from Eq. (4), assuming zero mean Gaussian distribution in both real and imaginary channels.

$$P_N = \frac{P_S}{10^{(\frac{SNR}{10})}} \tag{3}$$

$$SNR = 10\log_{10}\frac{P_S}{P_N} \tag{4}$$

where P_S and P_N denote the power of signal and noise, respectively. In a Gaussian process, the power of noise can be estimated from its variance δ^2, as nearly all the power in a Gaussian signal is contained within 3δ (three standard deviations). Noise was introduced into both the coil image and the uniform reference image in K-space to simulate the MR signal acquisition. The raw sensitivity profile is obtained by dividing the coil image by the uniform reference image in the image domain. Fig. 2C plots the results of adding 40 dB noise to the FEKO B_1 field (Fig. 2B).

According to Eq. (2), the optimization process can be described as follow:

$$\min_{\alpha,\gamma,I}[(\boldsymbol{B_v} - \boldsymbol{B}_1) \times (\boldsymbol{B_v} - \boldsymbol{B}_1)^H] \tag{5}$$

where subscript $\boldsymbol{v}$ represents a vector of points (40 points in the example shown in Fig. 2C) selected to describe the characteristics of the profile; $\boldsymbol{B_v}$ is the calculated magnetic field obtained by using Biot–Savart Law at vector $\boldsymbol{v}$ according to Eq. (6) [22,23]; and $\boldsymbol{B}_1$

stands for the complex-valued field strength in the noise-added profile at the same locations.

$$\boldsymbol{B}_v(\boldsymbol{V}_r) = \frac{\mu_0 \boldsymbol{I}}{4\pi} \oint_C \frac{\boldsymbol{dl}' \times \boldsymbol{R}}{\boldsymbol{R}^3} \tag{6}$$

In Eq. (6) the line integral is performed along the coil path C; vector $\boldsymbol{I}$ denotes the resonance current in the coil; vector $\boldsymbol{dl}'$ denotes the small increment of coil tangential to C; and $\boldsymbol{R}$ is the vector from $\boldsymbol{dl}'$ to the observation points. It is important to note that Eqs. (5) and (6) are determined by the descriptors of the mathematical model. In the optimization process, these descriptors, to which an appropriate amount of flexibility was given in order to accommodate any imperfection resulting from coil array manufacturing and uncertainties in the experiments, were the optimization variables. The optimized profile $\boldsymbol{B}_{\text{opt}}$ was obtained by substitution of the optimized values of those variables into Eq. (1). Fig. 3 illustrates the process of applying the proposed method to the scenario shown in Fig. 1. Fig. 3 depicts the coil image (A) and the homogeneous image (B) which were obtained as in the traditional method. The division (C) and masking (D) were performed as previously described. The extrapolation and polynomial fit was then replaced with the optimization process, which resulted in a set of optimized values of the descriptors. These descriptors were then used to calculate the sensitivity profile with a full field-of-view (FOV) (F).

The optimization was implemented in MATLAB (Mathworks, Natick, MA) using the subspace trust-region method based on the interior-reflective Newton method [24]. The evaluation of the error function involved the Biot–Savart integration which was programmed in C to reduce the computational time. The optimization converged within 100 iterations on average, using less than 30 seconds on an Intel Core 2 computer with 2 GB RAM.

To set up a fair comparison of the performance between the proposed method and the conventional method, both methods were optimized separately. An example of the conventional method is shown in Fig. 4. Reliable data points (depicted by blue dots in Fig. 4A) within a window of the raw sensitivity profile were incorporated into the polynomial fitting procedure to estimate the value at the centre of the area (depicted by a red dot in Fig. 4A and B).

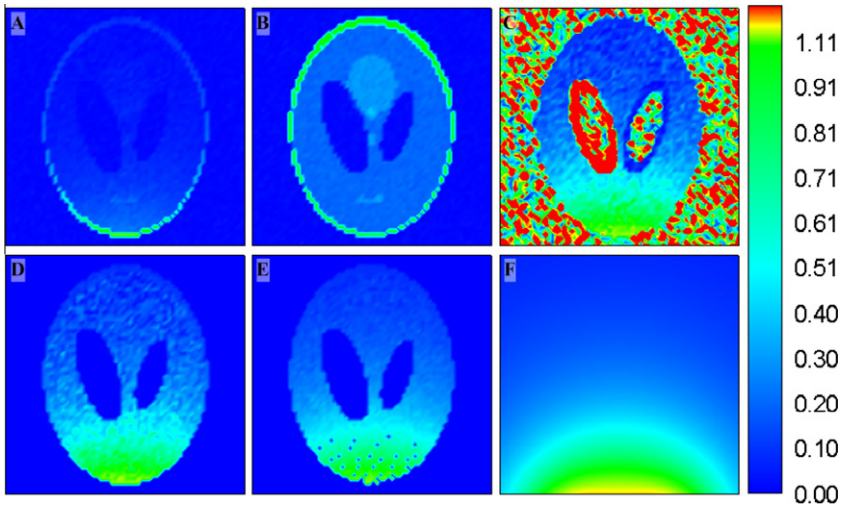

Fig. 3. The proposed coil sensitivity mapping procedure. The raw sensitivity profile (D) is obtained as depicted in Fig. 1. 30 points are selected on the raw sensitivity profile to best represent the characteristics of the profile (E). The optimization process is performed to acquire the variable values by minimizing the difference between the magnetic field of those 30 points calculated by Biot-Savart law and sensitivity values of those 30 points from E. Sensitivity profile (F) is then available by substitution, once variable values are determined.

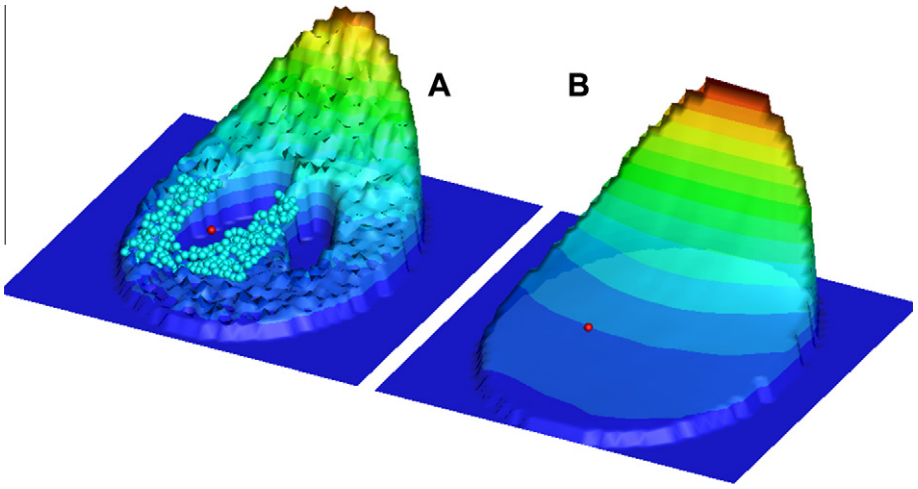

Fig. 4. The traditional polynomial fitting and extrapolation for the purpose of sensitivity map refinement. A set of data (blue dots) of raw sensitivity map (A) within a window are incorporated into polynomial fitting/extrapolation to estimate the value of the middle point of the window (red dot). This operation is repeated on the extrapolation zone (Fig. 1E) to obtain the refined sensitivity profile (B). (For interpretation of the references to colour in this figure legend, the reader is referred to the web version of this article.)

This example could be considered as a polynomial extrapolation, since the estimation point was outside the available data region. The fitting/extrapolation operated over the entire extrapolation zone (Fig. 1E) to acquire a fitted profile (Fig. 4B). The window size was made adaptable so that a sufficient amount of reliable data points were incorporated into the estimation. Higher order fitting to border regions was restricted [2].

Polynomial fittings were performed to acquire noise-reduced profiles $\boldsymbol{B}_{\text{poly}}$. $\boldsymbol{B}_{\text{opt}}$ denotes the sensitivity profile derived by the optimization process. The root mean square deviations (RMSD) of $(\boldsymbol{B}_{\text{opt}} - \boldsymbol{B}_1)$ and $(\boldsymbol{B}_{\text{poly}} - \boldsymbol{B}_1)$ were calculated to measure error amplitude when noise was introduced into the system. $\boldsymbol{B}_{\text{opt}}$ and $\boldsymbol{B}_{\text{poly}}$ were then used to reconstruct a phantom image using the SENSE method with a reduction factor of two ($R = 2$) and one-dimensional (1D) uniform under-sampling. The reconstruction results were examined against a visual inspection and a calculation of the artefact power.

2.3. Case II – multiple coil elements

In a more practical situation, multiple coil elements were used to acquire NMR signals simultaneously. An example of the four coil elements is shown in Fig. 5A. This coil geometry was obtained by expanding the configuration described in Fig. 2A – another three coils were placed at 90°, 180° and 270° with respect to the cylindrical coordinate system. Again, FEKO was used to model and simulate the magnetic field within the FOV. The coil element under inspection was driven by a unit-amplitude current source. The system was tuned to resonate at 64 MHz.

In this case, the principle of reciprocity still holds. The mutual induction between the primary coil and the ones within its vicinity is taken into account when creating the mathematical model. The inclusion of mutual coupling has to be reflected by adapting the function $\mathcal{F}_0$. The modified functional relationship can be described as:

$$\boldsymbol{B}' = \boldsymbol{B}_0 + \sum_i \boldsymbol{B}_i = \mathcal{F}_0(\gamma, \alpha, \bar{I}) + \sum_i \mathcal{F}_i(\gamma_i, \alpha_i, \bar{I}_i) \tag{7}$$

The net magnetic field $\boldsymbol{B}'$ characterising the sensitivity profile is considered to be the primary magnetic field $\boldsymbol{B}_0$ produced by the primary coil element, superimposed by magnetic field $\boldsymbol{B}_i$ produced by proximate coil elements driven by induced currents $\bar{I}_i$.

Similar to Eq. (5) for the single coil case, a optimization process is used to minimize

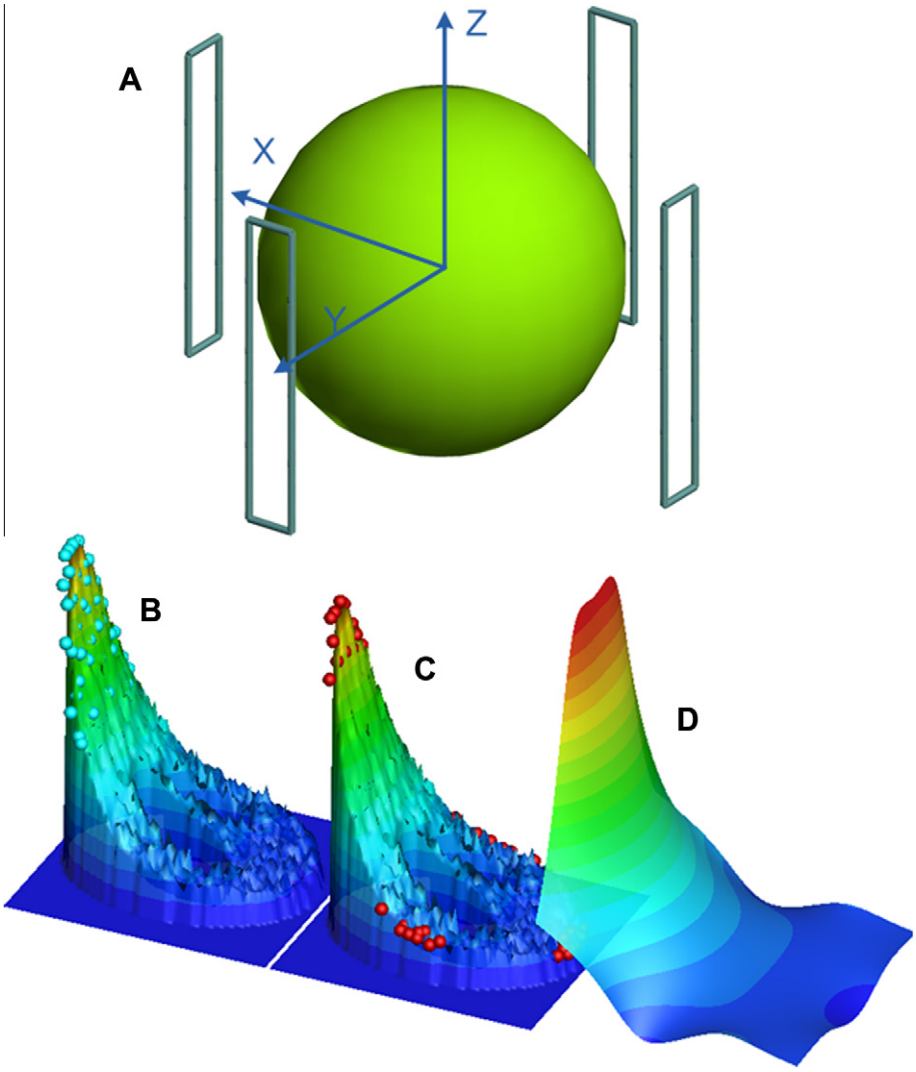

Fig. 5. (A): Geometry of an array of four coils. The field-of-field (FOV) sits in the centre slice of a spherical phantom (z = 0). Four elements are 90° apart. Noise-free sensitivity profile (B) is obtained from FEKO simulation according to geometry in (A). 30 dB noise added sensitivity Profile (C, D). Blue points in C are utilized to estimate the relative position of the primary coil under investigation. The yellow dots are employed to estimate the rest of the descriptors. (For interpretation of the references to colour in this figure legend, the reader is referred to the web version of this article.)

$$\min_{\alpha,\alpha_i,\gamma,\gamma_i,I,I_i}[(\boldsymbol{B}'_v-\boldsymbol{B}_1)\times(\boldsymbol{B}'_v-\boldsymbol{B}_1)^H] \tag{8}$$

Compared with Eq. (5), Eq. (8) employs $\boldsymbol{B}'_v$ to replace $\boldsymbol{B}_v$ to account for the mutual inductions among coils.

$$\boldsymbol{B}'^{(N)}_v=\frac{\mu_0 \boldsymbol{I}}{4\pi}\oint_C\frac{d\boldsymbol{l}'\times\boldsymbol{R}}{\boldsymbol{R}^3}+\sum_i\frac{\mu_0 \boldsymbol{I}_i}{4\pi}\oint_{C_i}\frac{d\boldsymbol{l}'\times\boldsymbol{R}}{\boldsymbol{R}^3} \tag{9}$$

The interrelationships of descriptors I, I_i, α, α_i, γ and γ_i can be taken into account in order to increase the accuracy and efficiency of the optimization. In general, the coil elements are uniformly distributed around the scanned subject and equidistant from the centre of the FOV. These relationships, the optimized constraints, can be mathematically described as: $\gamma_i=\gamma\pm v_i$ and $\alpha_i=\alpha+\frac{\pi}{2}\times i\pm\varepsilon_i$, where v_i and ε_i have small numerical values used to tolerate the imperfections of the coil fabrication process.

The optimization was executed in two stages. α was firstly determined by incorporating a few points that lie within the area where the primary coil element dominated (blue dots in Fig. 5B). With given ε_i, the lower and upper bounds of α_i were established accordingly. Having α determined and α_i constrained, a second stage optimized against the rest of the descriptors by minimizing Eq. (8), with sample points v selected around the edges of the profile (red dots in Fig. 5C). Once the values of all the descriptors were determined, they were substituted into Eq. (7) to acquire the coil sensitivity profile (Fig. 5D).

Similar to the examination described in Case I, polynomial fittings were performed for the performance comparison. The RMSD

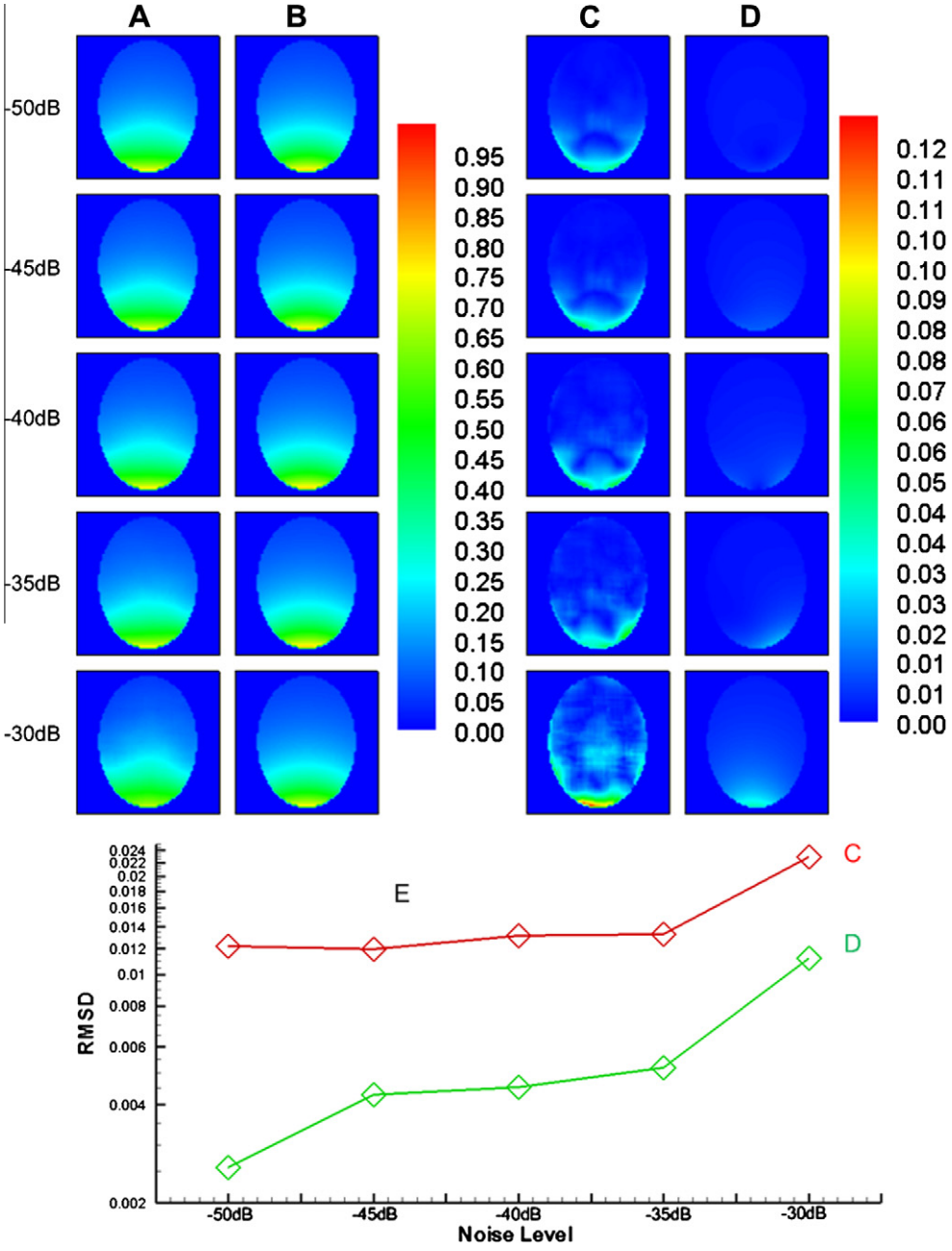

Fig. 6. Raw sensitivity maps are refined by polynomial fittings and extrapolations (A). Proposed method (B) is used to estimate sensitivity profiles from the same set of raw sensitivity maps. The error between estimations and noise-free profiles are shown for traditional polynomial refinement (C) and the proposed method (D). Root mean square deviation are assessed to compare the amplitudes of the sensitivity estimation errors (E).

of the profiles were calculated. SENSE reconstructions were performed using profiles from the polynomial fittings and the proposed method. The artefact power was then evaluated from the reconstruction.

3. Results

To evaluate the performance of the proposed method, we compared it with traditional methods in terms of the error amplitude of the sensitivity profile and the artefact power of the reconstructed image. The refined profiles of Case I were displayed in Fig. 6. The constructed sensitivity profiles using the conventional method (A) were compared to the proposed method (B) with the signal-to-noise ratio (SNR) ranging from 50 dB to 30 dB. It can be seen that the profiles obtained by polynomial fitting (A) show increased inhomogeneity and local distortions, as the noise level increased, whereas the profiles obtained by the proposed method remain undisturbed. This can be easily observed through Fig. 6C and D, which depict the difference between the original noise-free profiles and the constructed profiles. The RMSD were calculated against these differences to quantify the error amplitude as depicted in Fig. 6E. The proposed method produced sensitivity profiles with RMSD errors significantly less than those of the conventional method across the range of noise levels evaluated. In Fig. 7, the SENSE reconstructed images of the conventional method (A) and the proposed method (B) are shown. With SNR levels ranging from 50 dB to 30 dB, the proposed method produced images without any visible degradation, while the conventional

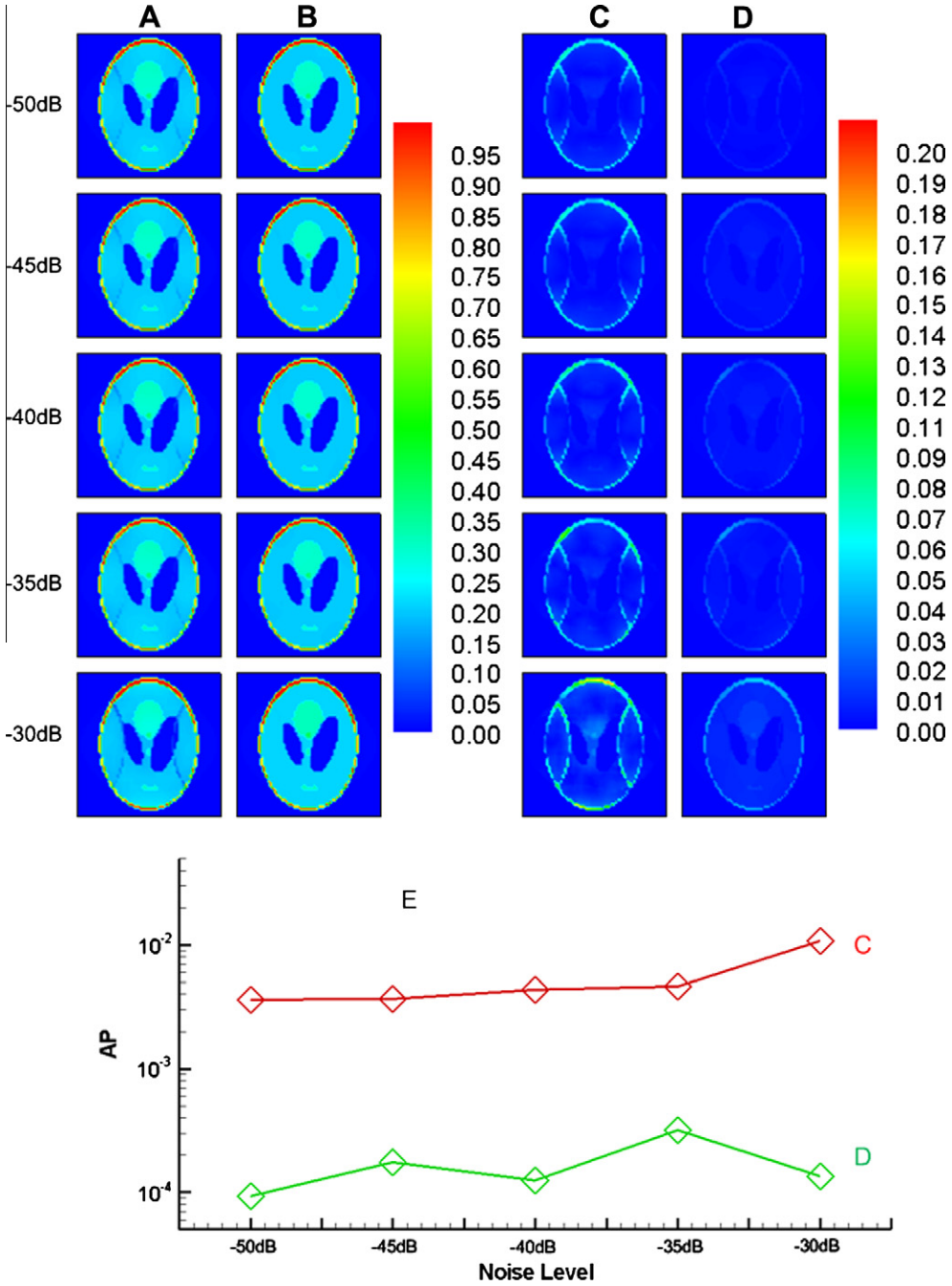

Fig. 7. SENSE reconstructions are performed with reduction factor 2, from profiles estimated by polynomial refinement (A) and proposed method (B). Error images (C and D) are derived between reconstructed images (A and B) and original image. Artefact power is calculated and compared to assess the reconstruction error quantitatively (E).

method generated visible artefacts at low SNR levels. Error images of the conventional method (7C) and the proposed method (7D) are provided. The reconstruction errors of the traditional method became more apparent when noise increased, while in contrast, the reconstruction error of the proposed method was only visible at high noise levels. Artefact power (AP), as shown in 7E, associated with the proposed method was at least an order of magnitude less than that of the conventional method.

In Case II, the same set of analyses was used to simulate the scenario where a set of four coils acquired data simultaneously. The results, shown in Figs. 8 and 9, are similar to those in Case I, which indicate that the optimization process, described by Eq. (7) and Fig. 5, successfully constructed coil sensitivity profiles in the presence of mutual coupling. In Fig. 9D we can see that the superior sensitivity estimations yielded reconstructions with considerably less visible artefacts over the SNR levels evaluated, while artefacts obtained by the conventional method were noticeable at low SNR levels as seen in Fig. 9C. The advantage of the proposed method, over the conventional method, was quantitatively justified by the calculation of artefact power (Fig. 9E). Similar to Case I, the artefact power of the proposed method was more than an order of magnitude less than that of the traditional method.

4. Discussion and conclusion

In order to reduce noise in sensitivity map estimations and consequently improve the SENSE reconstructions, a novel framework

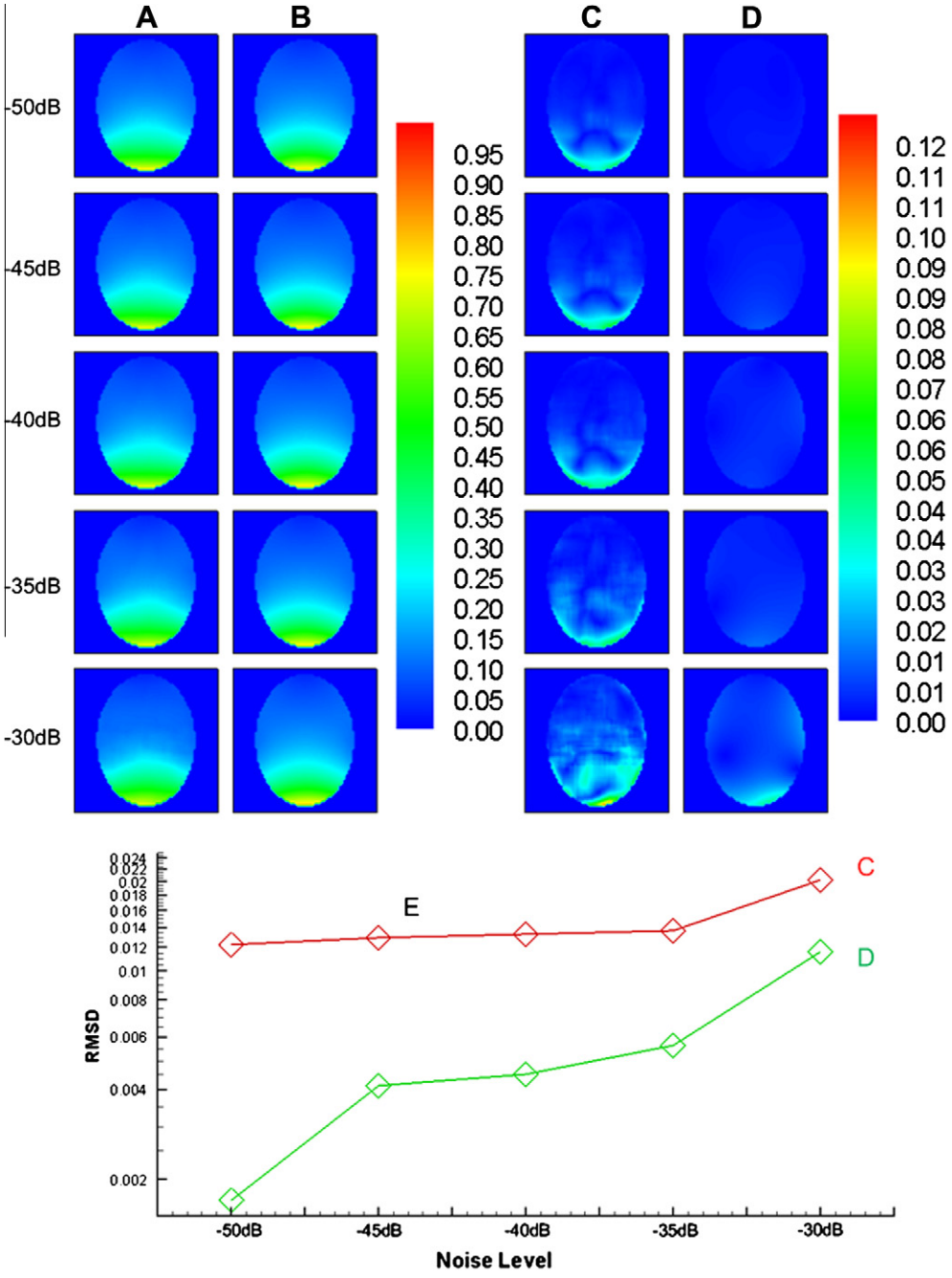

Fig. 8. Raw sensitivity maps are refined by polynomial fittings and extrapolations (A) and the proposed method (B) the error between estimations and noise-free profiles are shown for traditional polynomial refinement (C) and the proposed method (D). Root mean square deviation are assessed to compare the amplitudes of the sensitivity estimation errors (E).

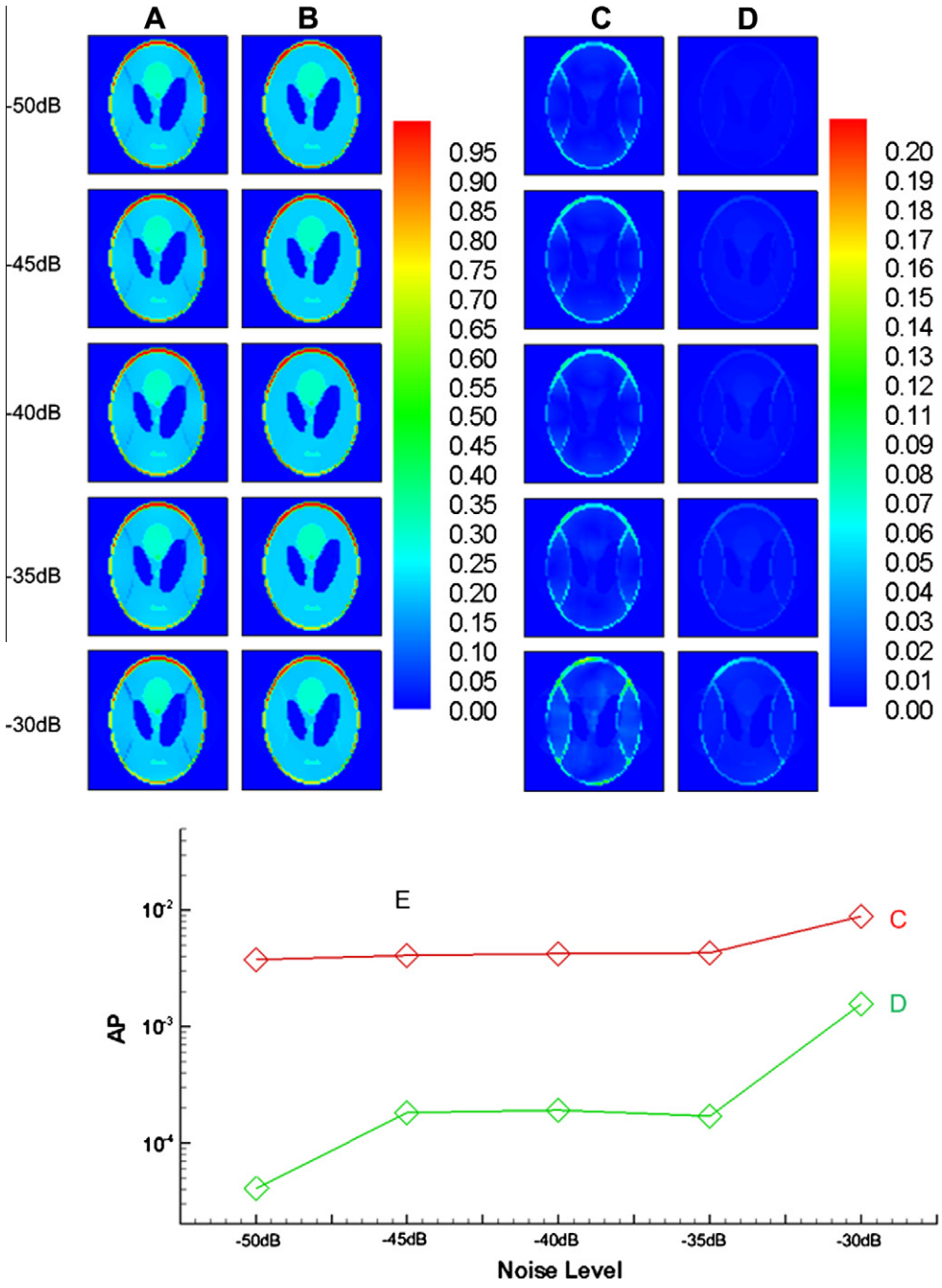

Fig. 9. SENSE reconstructions are performed with reduction factor 2, from profiles estimated by polynomial refinement (A) and the proposed method (B). Error images (C and D) are derived between reconstructed images (A and B) and the original image. Artefact power is calculated and compared to assess the reconstruction error quantitatively (E).

of sensitivity mapping was introduced. Instead of determining sensitivity by refining raw sensitivity profiles using polynomial fitting or other signal processing techniques, such as wavelet de-noising, the raw profiles were fitted to a B_1 field of a coil array. The only prerequisite for the implementation of the proposed method was the approximate knowledge of the coil geometry. The proposed method was investigated using two scenarios at 1.5T. Case I demonstrated this novel method in the simplest form, whereas Case II dealt with sensitivity mapping for multiple receiver coils. In each case, a mathematical model was established according to the prior knowledge of the coil array and governing electromagnetics. An optimization algorithm was then employed to search for a B_1 field, with the least discrepancies with the raw sensitivity profile.

Since the proposed method is a method of refining raw sensitivity maps, it is suitable for scenarios where a reference scan is available (static sensitivity mapping), as well as the cases where a raw sensitivity profile is estimated from the central K-space (dynamic sensitivity mapping). Furthermore, it is not subject to Gibbs ringing, a problem specific to the dynamic methods, because the optimized profile is numerically obtained from the physics of electromagnetics. The results shown in Section 3 indicates that the proposed method was able to obtain sensitivity profiles with lower noise amplitude, which favours the SENSE reconstructions in terms of less artefact power for the reconstructed images.

The current method only addresses the low-field scenarios. At high-fields (HF), the RF wavelength becomes close to or shorter

than the anatomy being scanned and the geometry of the RF coil. The loading effects and coil-tissue interactions lead to non-uniform distributions of the RF current in the coil [25–28]. These effects are no longer negligible and invalidate the use of Biot–Savart Law for the calculation of the B_1 fields at HFs and it requires full-wave electromagnetic solutions. In these cases, a detailed RF coil model has to be developed to consider the variations of RF currents (including amplitudes and phases) and array coupling; fortunately, hybrid numerical approaches [27,28] can be used to handle the involved electromagnetic problem. In addition, the HF B_1^+ and B_1^- behave differently and therefore caution should be exercised when relating the reception sensitivity to the transmission sensitivity of the same coil using the reciprocity theorem. Currently we are working on extending the proposed concept for HF applications including parallel reconstruction and parallel transmission [29–32].

References

[1] F. Wiesinger, P.F. Van de Moortele, G. Adriany, N. De Zanche, K. Ugurbil, K.P. Pruessmann, Potential and feasibility of parallel MRI at high field, NMR in Biomedicine 19 (2006) 368–378.

[2] K.P. Pruessmann, M. Weiger, M.B. Scheidegger, P. Boesiger, SENSE: sensitivity encoding for fast MRI, Magnetic Resonance in Medicine 42 (1999) 952–962.

[3] K.P. Pruessmann, M. Weiger, P. Bornert, P. Boesiger, Advances in sensitivity encoding with arbitrary k-space trajectories, Magnetic Resonance in Medicine 46 (2001) 638–651.

[4] M.A. Griswold, P.M. Jakob, R.M. Heidemann, M. Nittka, V. Jellus, J.M. Wang, B. Kiefer, A. Haase, Generalized autocalibrating partially parallel acquisitions (GRAPPA), Magnetic Resonance in Medicine 47 (2002) 1202–1210.

[5] M.A. Griswold, P.M. Jakob, M. Nittka, J.W. Goldfarb, A. Haase, Partially parallel imaging with localized sensitivities (PILS), Magnetic Resonance in Medicine 44 (2000) 602–609.

[6] W.E. Kyriakos, L.P. Panych, D.F. Kacher, C.F. Westin, S.M. Bao, R.V. Mulkern, F.A. Jolesz, Sensitivity Profiles from an Array of Coils for Encoding and Reconstruction in Parallel (SPACE RIP), John Wiley & Sons Inc., Denver, Colorado, 2000. pp. 301–308.

[7] P.M. Jakob, M.A. Grisowld, R.R. Edelman, D.K. Sodickson, AUTO-SMASH: a self-calibrating technique for SMASH imaging, Magnetic Resonance Materials in Physics, Biology and Medicine 7 (1998) 42–54.

[8] M.A. Griswold, P.M. Jakob, Q. Chen, J.W. Goldfarb, W.J. Manning, R.R. Edelman, D.K. Sodickson, Resolution enhancement in single-shot imaging using simultaneous acquisition of spatial harmonics (SMASH), Magnetic Resonance in Medicine 41 (1999) 1236–1245.

[9] R.M. Heidemann, M.A. Griswold, A. Haase, P.M. Jakob, VD-AUTO-SMASH imaging, Magnetic Resonance in Medicine 45 (2001) 1066–1074.

[10] D.K. Sodickson, C.A. McKenzie, A generalized approach to parallel magnetic resonance imaging, Medical Physics 28 (2001) 1629–1643.

[11] Z. Chen, J. Zhang, R. Yang, P. Kellman, L.A. Johnston, G.F. Egan, IIR GRAPPA for parallel MR image reconstruction, Magnetic Resonance in Medicine 63 (2009) 502–509.

[12] W.S. Hoge, D.H. Brooks, Using GRAPPA to improve autocalibrated coil sensitivity estimation for the SENSE family of parallel imaging reconstruction algorithms, Magnetic Resonance in Medicine 60 (2008) 462–467.

[13] C.A. McKenzie, E.N. Yeh, M.A. Ohliger, M.D. Price, D.K. Sodickson, Self-calibrating parallel imaging with automatic coil sensitivity extraction, Magnetic Resonance in Medicine 47 (2002) 529–538.

[14] F.H. Lin, Y.J. Chen, J.W. Belliveau, L.L. Wald, A wavelet-based approximation of surface coil sensitivity profiles for correction of image intensity inhomogeneity and parallel imaging reconstruction, Human Brain Mapping 19 (2003) 96–111.

[15] L. Ying, J. Sheng, Joint Image reconstruction and sensitivity estimation in SENSE (JSENSE), Magnetic Resonance in Medicine 57 (2007) 1196–1202.

[16] D.I. Hoult, The principle of reciprocity in signal strength calculations – a mathematical guide, Concepts in Magnetic Resonance Part A 12 (2000) 173–187.

[17] T.S. Ibrahim, Analytical approach to the MR signal, Magnetic Resonance in Medicine 54 (2005) 677–682.

[18] P.B. Roemer, W.A. Edelstein, C.E. Hayes, S.P. Souza, O.M. Mueller, The NMR phased-array, Magnetic Resonance in Medicine 16 (1990) 192–225.

[19] J.M. Wang, A. Reykowski, J. Dickas, Calculation of the signal-to-noise ratio for simple surface coils and arrays of coils, IEEE Transactions on Biomedical Engineering 42 (1995) 908–917.

[20] F. Liu, A. Trakic, H.S. Lopez, Q. Wei, M. Fuentes, E. Weber, S. Crozier, Reverse-engineering of gradient coil designs based on experimentally measured magnetic fields and approximate knowledge of coil geometry-application in exposure evaluations, Concepts in Magnetic Resonance Part B: Magnetic Resonance Engineering 35B (2009) 32–43.

[21] M.A. Griswold, F. Breuer, M. Blaimer, S. Kannengiesser, R.M. Heidemann, M. Mueller, M. Nittka, V. Jellus, B. Kiefer, P.M. Jakob, Autocalibrated coil sensitivity estimation for parallel imaging, NMR in Biomedicine 19 (2006) 316–324.

[22] J.D. Jackson, Classical Electrodynamics, 3rd ed., Wiley, New York, 1925.

[23] D.K. Cheng, Field and Wave Electromagnetics, second ed., Addison-Wesley, Pub Co, Berlin, 1917.

[24] T.F. Coleman, Y. Li, An interior trust region approach for nonlinear minimization subject to bounds, SIAM Journal on Optimization 6 (1996) 418–445.

[25] T.S. Ibrahim, R. Lee, B.A. Baertlein, Y. Yu, P.M.L. Robitaille, Computational analysis of the high pass birdcage resonator: finite difference time domain simulations for high-field MRI, Magnetic Resonance Imaging 18 (2000) 835–843.

[26] T.S. Ibrahim, C. Mitchell, R. Abraham, P. Schmalbrock, In-depth study of the electromagnetics of ultrahigh-field MRI, NMR in Biomedicine 20 (2007) 58–68.

[27] F. Liu, B.L. Beck, B. Xu, J.R. Fitzsimmons, S.J. Blackband, S. Crozier, Numerical modeling of 11.1T MRI of a human head using a MoM/FDTD method, Concepts in Magnetic Resonance Part B: Magnetic Resonance Engineering 24B (2005) 28–38.

[28] F. Liu, S. Crozier, Electromagnetic fields inside a lossy. Multilayered spherical head phantom excited by MRI coils: models and methods, Physics in Medicine and Biology 49 (2004) 1835–1851.

[29] W.A. Grissom, C.Y. Yip, S.M. Wright, J.A. Fessler, D.C. Noll, Additive angle method for fast large-tip-angle RF pulse design in parallel excitation, Magnetic Resonance in Medicine 59 (2008) 779–787.

[30] D. Xu, K.F. King, Y.D. Zhu, G.C. McKinnon, Z.P. Liang, A noniterative method to design large-tip-angle multidimensional spatially-selective radio frequency pulses for parallel transmission, Magnetic Resonance in Medicine 58 (2007) 326–334.

[31] Y. Zhu, Parallel excitation with an array of transmit coils, Magnetic Resonance in Medicine 51 (2004) 775–784.

[32] U. Katscher, P. Bornert, C. Leussler, J.S. Van den Brink, Transmit SENSE, Magnetic Resonance in Medicine 49 (2003) 144–150.